Nuclear Engineering and Design 37 (1976) 333–346

STRUCTURAL ANALYSIS OF AIRCRAFT IMPACT ON A NUCLEAR POWERED SHIP

R. DIETRICH

Institut für Anlagentechnik, Gesellschaft für Kernenergieverwertung in Schiffbau und Schiffahrt mbH., D-2054 Geesthacht-Tesperhude, Germany

Received 15 December 1975

As part of a general safety analysis, the reliability against structural damage due to an aircraft crash on a nuclear powered ship is evaluated. This structural analysis is an aid in safety design. It is assumed that a Phantom military jet-fighter hits a nuclear powered ship. The total reaction force due to such an aircraft impact on a rigid barrier is specified in the guidelines of the Reaktor-Sicherheitskommission (German Safety Advisory Committee) for pressurized water reactors.

This paper investigates the aircraft impact on the collision barrier at the side of the ship. The aircraft impact on top of the reactor hatchway is investigated by another analysis. It appears that the most unfavorable angle of impact is always normal to the surface of the collision barrier. Consequently, only normal impact will be considered here. For the specific case of an aircraft striking a nuclear powered ship, the following two effects are considered: Local penetration and dynamic response of the structure.

The local penetration occurs at points where the engines or other rigid objects hit the structure. It is assumed that the aircraft engine is a rigid body projectile and the side wall of the ship is the target. The applied steel penetration formulae for projectiles were empirically derived for military applications, where both the projectile and the target are unlike those of an impact of an aircraft engine. For this reason it is expedient to calculate the upper and the lower limit values of the penetration depths. The results show that the highest penetration depth is less than the sum of all wall thicknesses of the collision barrier.

The solution of the dynamic analysis is obtained by using the finite element method. The results are the eigenmodes, the eigenfrequencies, the displacements of the nodes, and the stresses in the applied plane stress elements. It is shown that the maximum stress which only appears in one element is on the same level as the yield stress of the St. 42 steel. The structural analysis shows that the collision barrier is a sufficient safeguard against the perforation of the engine and against the cracking of the structure as a result of the dynamic response to an aircraft impact.

1. Introduction

The impact of an aircraft on a nuclear 80 000 shp container ship (NCS 80) is investigated to analyse the safety of such a ship against external impact loads. The reactor plant must be protected against impact damage because the surrounding environment must be subjected to the consequences of such an impact. The collision barrier must protect the reactor plant and ensure that an impact due to an aircraft striking the side wall as well as the upper deck will not cause any damage.

On both sides of the ship there is a collision barrier structure which protects the reactor plant against ship collision. This collision barrier also provides protection against horizontal aircraft impacts. The upper deck does not have such an elaborate collision protection structure. However, the deck plating covering the auxiliary machinery is stiffened or supported by transverse and longitudinal bulkheads. The hatch cover above the reactor is built as a grid structure in the same way as the collision protection at the sides of the ship.

This paper investigates an aircraft impact on the collision barrier at the side of the ship (see fig. 1). The aircraft impact on top of the reactor hatchway is investigated by another analysis.

* Paper S2/6 presented at the International Seminar on Extreme Load Conditions and Limit Analysis Procedures for Structural Reactor Safeguards and Containment Structures (ELCALAP), Berlin, Germany, 8–11 September 1975.

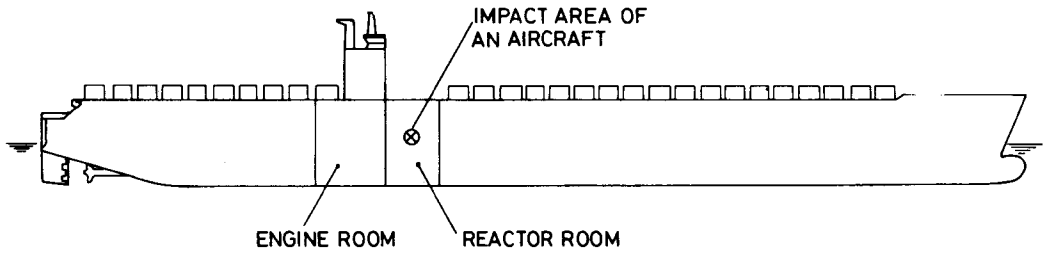

Fig. 1. Side view.

2. General assumptions

An aircraft impact on a structure causes a dynamic load on a finite area. The localized pressure can be distributed unevenly over this impact area. However, the distribution of this impact load is not known, and for this reason this investigation only considers a uniformly distributed pressure over the impact area.

The stresses in the structure are not only dependent on the distribution of the impact load, but also on the design of the structure, the assumed impact loads, the dynamic response of the structure as well as the scantlings of the structural plating.

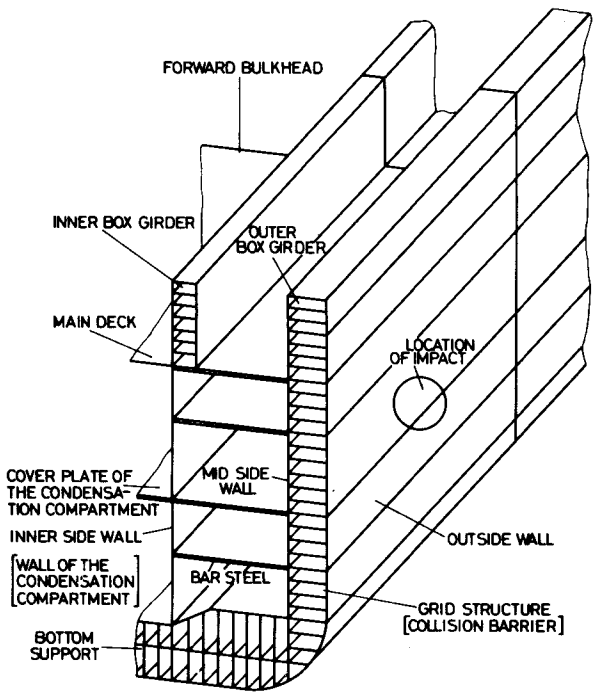

Fig. 2. Cross section of reactor compartment.

2.1. Structural design of the collision barrier

The collision barrier, located at the sides of the reactor compartment, is a complex orthogonal structure. Fig. 2 shows a cross section of the structural configuration of the reactor compartment.

2.2. Impact loads

The assumptions of the impact area, impact angle and impact load time function are based on specifications of the guidelines of the Reaktor-Sicherheitskommission (German Reactor Safety Advisory Committee) for pressurized water reactors (PWRs). The size of the impact area is specified as 7 m^2. The impact area is assumed to be located at the center of the collision barrier of the ship's side because maximum stresses in this structure can be expected for this condition. The

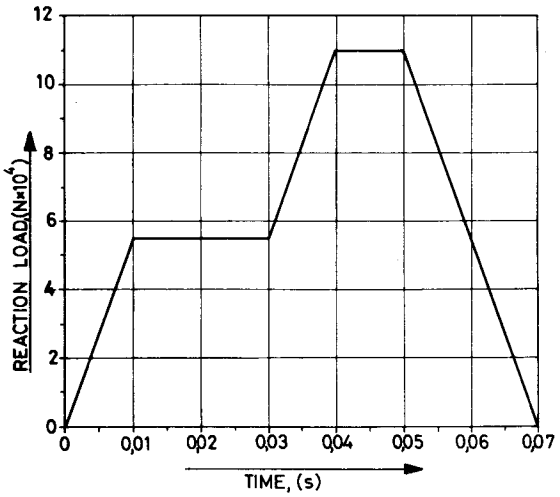

Fig. 3. Reaction load versus time of impact for a military jet fighter Phantom on a rigid wall [1].

angle of impact is assumed to be normal to the surface of the collision barrier because this is the most unfavorable condition. The impact load time function is assumed as shown in fig. 3 and corresponds to an impact of a Phantom military jet-fighter having a strike velocity of 774 km/hr [2,3].

2.3. Dynamic response of the structure

The dynamic response of the structure and the resulting stresses are based on linear–elastic behaviour of the material. This allows the localization of possible areas of plastic deformations. Hence, a dynamic analysis can be carried out if necessary, considering these local areas of plastic deformation.

2.4. Scantlings of the structure (fig. 2)

Outside wall thickness [6]: 33 mm *; mid side wall thickness [5]: 20 mm; and inner side wall thickness [5]: 23 mm.

2.5. Grid structure

The distance between the grid plates in the y direction [5]: 775 mm; distance between the grid plates in the z direction [5]: 880 mm; thickness of the grid plates [5]: 18 mm; and distance between the outside wall and the mid side wall [5]: 2300 mm.

2.6. Decks

Thickness [5]: 18 mm; cross-sectional area of the bar steels [5]: 8940 mm^2; cross-sectional area of the bar steels of the forward and aft transverse bulkhead [6]: 89400 mm^2; distance between the bar steels [5]: 775 mm; and distance between the mid side wall and the inner side wall [5]: 7300 mm.

3. Calculations performed

The impact of an aircraft on the side structure of a ship effects the structural strength, the penetration phenomena and the dynamic response.

* Wall thickness has been increased to 38 mm because of ship structural considerations. The outer wall thickness of 38 mm is used for calculation of the penetration depth.

3.1. Penetration phenomena

Penetration phenomena are caused mainly by compact parts of the aircraft which separate themselves from the aircraft before or during impact and strike the ship structure. The impact of an engine is a special danger because it represents a compact concentration of a relatively large mass (approximately 1740 kg) [3, 4] within a small volume. In case of frontal impact the engine (diameter approximately 1 m [4]) behaves as a projectile and can penetrate or perforate the structure. The penetration depth of the ship's side structure is of particular interest in this investigation.

Assuming the aircraft engine acts as a striking projectile and the outside wall of the ship acts as a rigid steel plate, the empirically derived ballistic relationships for the determination of penetration depth can be used.

In this investigation modified forms of the empirically derived BRL equation (Ballistic Research Laboratories equation) [16] and the RM equation (Rheinmetall equation) [15] are used as follows:

BRL equation

$$T = K_{\mathrm{BRL}} \frac{G^{0.67}}{D} \left(\frac{v}{100}\right)^{1.33}, \tag{1}$$

RM equation

$$T = K_{\mathrm{RM}} \frac{G^{0.71}}{D^{1.07}} \left(\frac{v}{100}\right)^{1.43}, \tag{2}$$

where T is the steel plate thickness (m), G is the weight of the projectile (kp), D is the diameter of the projectile (m), v is the velocity of the projectile (km/hr), K_{BRL}, K_{RM} are the empirical coefficients to take into consideration the construction of the projectile and the properties of the material of the struck steel plate. The magnitudes of these coefficients are: $K_{\mathrm{BRL}} = 4.16 \times 10^{-5}$, $K_{\mathrm{RM}} = 1.37 \times 10^{-5}$ for solid-type missiles, $= 3.13 \times 10^{-5}$ for hard core-type missiles. Note that both equations are of the same kind, only their empirical exponents and coefficients are different.

Using these ballistic relationships the penetration depth results in a value which is too great because an aircraft engine during impact does not behave ballistically as a missile or a bomb. According to eq. (2), the penetration depth into a rigid steel plate is a function of not only the impact velocity, the diameter and

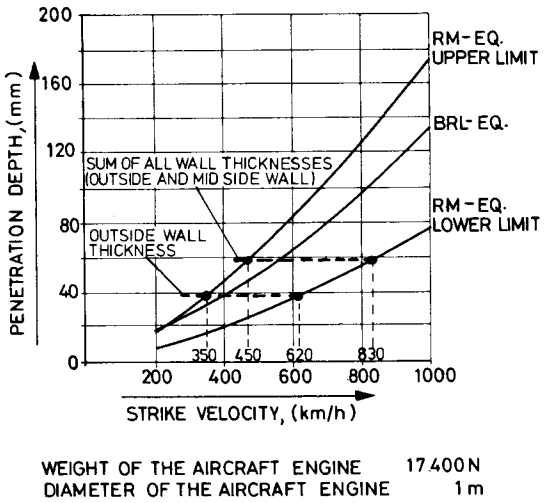

Fig. 4. Penetration depth of a projectile during impact on a steel plate. (Dimensions and weight of the projectile correspond to an engine of a Phantom aircraft.)

the mass, but also the construction and material properties of the projectile and the struck steel plate. Thus, an upper and a lower value are specified for the coefficient K resulting in an upper and a lower value of penetration depth.

Fig. 4 shows the penetration depth of a projectile as a function of impact velocity, determined by using eqs. (1) and (2). Dimensions and weight of the projectile correspond to an engine of a 'Phantom' aircraft. The values of penetration depth as a function of strike velocity as determined using the BRL equation (eq. (1)) have magnitude between the upper and lower limit values as determined using the RM equation (eq. (2)).

Using these curves for the determination of penetration depth during impact of an engine on the rigid steel plate, the maximum impact velocity for the upper curve is approximately 350 km/hr and for the lower curve approximately 620 km/hr assuming the wall thickness of 38 mm. This wall thickness corresponds to the outside wall thickness of NCS 80.

Including the protection of the mid side wall (see fig. 2) of 20 mm thickness, the magnitudes of impact velocities are increased to (a) approximately 450 km/hr for the upper curve, and (b) approximately 830 km/hr for the lower curve. For strength calculations of the impact of an aircraft engine on the collision barrier of a ship the values of the lower curve can be used as applicable because

(a) as mentioned above, an engine does not behave ballistically in the same way as a missile or a bomb;

(b) the outside and the mid side wall (see fig. 2) of the NCS 80 are structurally supported by the grid structures of the collision barrier where the horizontal and vertical distances (horizontal 0.775 m, vertical 0.880 m) between grid plates are less than the diameter of an aircraft engine (approximately 1 m); and

(c) the reduction of kinetic energy of the engine due to deformations of the grid plates can not be considered for lack of empirical data.

In addition it must be considered that the impact velocity of an aircraft engine is less than the impact velocity of an aircraft. According to the IRS [3] the impact velocity of an engine of a striking aircraft can be assumed to be approximately 360 km/hr. For this impact velocity the use of the upper, more pessimistic, curve (450 km/hr) provides a magnitude for the penetration depth which shows that the collision barrier is a sufficient safeguard against the perforation of an engine.

3.2. Dynamic analysis

During impact of an aircraft on the side structure of a ship, the load is time dependent and concentrated over the impact area. For strength calculations a dynamic analysis is necessary which takes into consider-

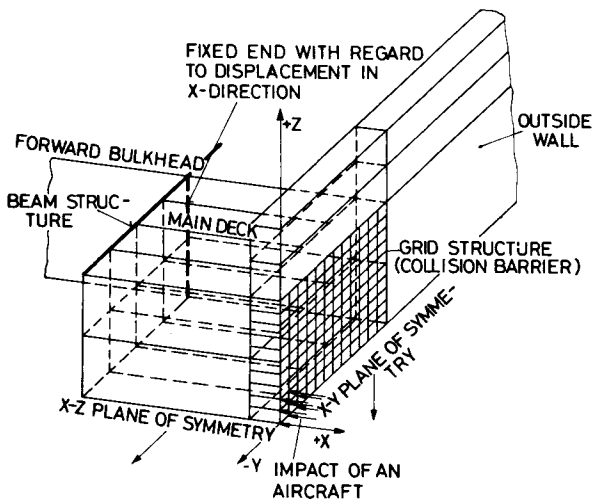

Fig. 5. Schematic of analysed structure.

ation the structure surrounding the impact location in order to accurately include the force distribution and energy loss due to the inertia of the surrounding structure. This often makes the analysis very time and cost intensive.

Comparing the mass of the struck ship with that of the striking aircraft, there results a ratio of approximately

$$M_{\text{aircraft}} : M_{\text{ship}} \approx 1 : 3000 \,. \tag{3}$$

This large ratio and the rapid reduction of the stresses at increasing distances from the impact area make it unnecessary to include the entire ship in the analysis. Therefore, the area to be analyzed can be localized whereby the boundary conditions must be chosen such that the calculated results are always conservative. The selection of the idealized model is based on these considerations.

3.2.1. Idealized model

The idealized model is shown in fig. 5 and is based on the ship's structure as shown in fig. 2. Only a quarter of the ship's side structure is included in this idealized model because the impact area is located at the symmetrical center of the ship's side structure. This reduces analysis computing time and manpower. However, the stiffness of the bottom cannot be fully taken into account due to the symmetry about the x–y plane (see fig. 2).

The supporting effect of the cover plate of the condensation compartment (see fig. 2) and the decks above and below this cover plate are not included. Consequently the structure is only fixed and supported at the transverse bulkhead. These assumptions are made because the purpose of this first investigation is to determine the maximum stresses in the collision structure. The distance between the individual decks are assumed equal. The scantlings of individual plates of the structure are given in subsection 2.4.

3.2.2. Methods used

The nodal point equilibrium equation for a system of structural elements can be derived from several approaches [7,13]. All methods yield a set of equations of motion of the following form:

$$M\ddot{x} + C\dot{x} + Kx = R(t) \,, \tag{4}$$

where M is the mass matrix; C is the damping matrix; K is the stiffness matrix of the element assemblage; $R(t)$ is the vector for the time-dependent external load; x is the vector for the nodal displacements; $\dot{x}$ is the vector for the nodal velocities; and $\ddot{x}$ is the vector for the nodal accelerations.

An analytical solution of the motion equations (4) of the present problem is not possible. However, a numerical solution of these equations can be obtained if the finite element method [7] is used. In this case the structure is first idealized into an assembly of structural elements and these elements are attached to the adjacent elements at node points, which may be either the actual joints or fictitious points obtained by the intersecting grid lines. To determine stiffness characteristics of the entire assembled structure which are required in the analysis, the stiffness properties of individual unassembled elements must be specified. Because for the present problem the plate elements of the grid structure (collision barrier) and of the decks are loaded by in-plane forces, plane stress elements are used for the idealization. For the idealization of the bar steels underneath the decks and of the inner box girder (fig. 2) the bar element ('truss' element) and the beam element are used, respectively. Based on this idealization and the scantlings of the structure the individual matrices are determined.

3.2.2.1. Eigenvalue problem. The free vibration properties of the finite element idealization may be evaluated by considering the equation of motion (eq. (4)) for the special case where the damping and external loads vanish:

$$R(t) = 0 \,, \qquad C = 0 \,. \tag{5}$$

Hence eq. (4) gives

$$M\ddot{x} + Kx = 0 \,. \tag{6}$$

In this case, the displacement shapes remain constant and their amplitudes vary harmonically, i.e. the displacement vector may be expressed as

$$x = \varphi \sin(\omega/t) \,. \tag{7}$$

Introducing eq. (7) into eq. (6) leads to

$$K\varphi = \omega^2 M\varphi \,, \tag{8}$$

in which ω and φ are the free vibration frequency and the mode shape, respectively. The n eigenvalues give

the natural frequencies of the system and the eigenvectors are the corresponding vibration modes. The complete solution to eq. (8) can be written

$$K\Phi = M\Phi\Omega^2 , \tag{9}$$

in which the columns in Φ are the corresponding M orthonormalized eigenvectors φ_i, and Ω^2 is a diagonal matrix with the n smallest eigenvalues:

$$\Omega^2 = \text{diag}\,(\omega_i^2) . \tag{10}$$

Two different solution procedures can be used, namely a determinant search technique or a subspace iteration solution. The determinant search solution is carried out if the stiffness matrix can be put into one high-speed storage block of the computer. Therefore, for systems of large order and bandwidth the subspace iteration method is used. Both solution techniques solve the generalized eigenvalue problem directly without a transformation to standard form [10].

3.2.2.2. Response to dynamic loading. The dynamic response analysis of a finite element system is performed by solving the equations of motion (eq. (4)). Two different techniques are available: the mode superposition method and the step-by-step integration.

The basic concept of the mode superposition method is that the displacement vector x can be expressed as a linear combination of vibration mode shapes:

$$x = \Phi X , \tag{11}$$

in which the columns in Φ are the corresponding M orthonormalized eigenvectors and X represents the vector of modal amplitudes. Introducing eq. (11) into the equations of motion (eq. (4)) leads to

$$\ddot{X} + \Lambda\dot{X} + \Omega^2 X = \Phi^{\mathrm{T}} R(t) , \tag{12}$$

in which Λ is the diagonal matrix ($\Lambda = \text{diag}\,(2\omega_i \cdot \xi_i)$) and ξ_i is the damping ratio in the ith mode of vibration.

This method is advantageous if the essential dynamic response of the structure is contained in the first few mode shapes. This will be the case if the applied load can be approximated reasonably well by inertia force patterns associated with the first few modes and if the frequency content of the input is largely represented by the corresponding lowest frequencies. For cases where the applied load distribution is extremely complex, and/or the time variation contains significant high frequency components, it will be necessary to include many modes of vibration to obtain adequate accuracy by mode superposition [14].

In this case, the step-by-step procedure may be more efficient [11,12]. To carry out a step-by-step solution of the simultaneous equations of motion the response history is divided into a sequence of time increments of equal length Δt. The equation of motion is formulated on an incremental basis and the motion computed during each time increment is added to the conditions at the beginning of the increment to obtain the conditions at the end. With this procedure the response is evaluated step-by-step throughout the desired time range, starting with any given initial condition. The incremental form of the equations of motion is

$$M^{t+\Delta t}\ddot{x} + C^{t+\Delta t}\dot{x} + Kx = {}^{t+\Delta t}R(t) , \tag{13}$$

where ${}^{t+\Delta t}\dot{x}$, ${}^{t+\Delta t}\ddot{x}$ are vectors of nodal point velocities and accelerations at time t; x is a vector of nodal point displacement increments from time t to time $t + \Delta t$ and Δt is the time increment.

If the analysis is done by the step-by-step method, the high frequency components will be included in the analysis. Moreover, direct step-by-step integration must be employed in any case if the structural response is nonlinear due to either material property or geometry effects. In this case C and K represent the effective damping and stiffness matrices, respectively, applicable during the time increment. These properties may be changing as the structure responds but it is reasonable to assume that they will remain constant during each time increment if the increments are made short enough.

The only other assumption introduced in the analysis is that the acceleration varies linearly during the time increment, which leads to expression for the change in velocity and acceleration in terms of the initial conditions and the change of displacement [14]. To do the numerical calculations the digital computer program SAP IV is used [9]. The number of elements and the degrees of freedom of the nodal points lead to a system of equations with 1145 unknown variables.

3.2.3. Results

A part of the dynamic analysis of the ship's side structure is the determination of the eigenvalues (eigenmodes and eigenfrequencies) and the dynamic response of the idealized structure due to dynamic loading.

3.2.3.1. Eigenvalues. To solve the eigenvalue problem (eq. (9)) the computer program SAP IV [10] is used. In this investigation only the first six mode shapes are determined. The first six eigenfrequencies are: (1) $f_1 = 23.8$ Hz; (2) $f_2 = 34.7$ Hz; (3) $f_3 = 49.3$ Hz; (4) $f_4 = 52.7$ Hz; (5) $f_5 = 71.5$ Hz; and (6) $f_6 = 71.7$ Hz. The eigenmodes corresponding to the first five eigenfrequencies are shown in fig. 6.

Using the time during impact of $T_I = 0.07$ sec (see fig. 3) the following ratio can be defined:

$$\alpha_i = \frac{1}{2 f_i T_I} = \frac{T_i/2}{T_I}, \tag{14}$$

in which T_i is the natural period ($T_i = 1/f_i$). The magnitudes of this ratio for the first six eigenfrequencies are: (1) $\alpha_1 = 0.30$; (2) $\alpha_2 = 0.21$; (3) $\alpha_3 = 0.15$; (4) $\alpha_4 = 0.14$; (5) $\alpha_5 = 0.10$; and (6) $\alpha_6 = 0.09$.

All values of α are less than 1 ($\alpha_i < 1$). Consequently the time during impact is larger than half the natural period (see eq. (14)) and thus a dynamic response of the ship's side structure is possible.

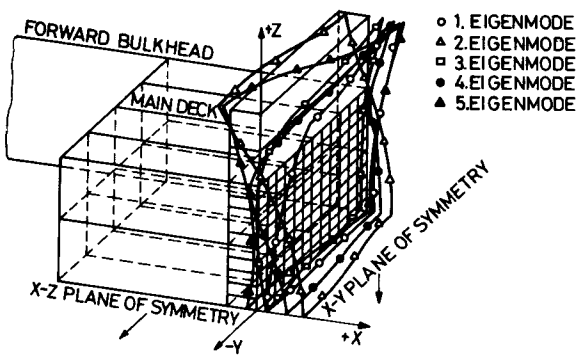

Fig. 6. Eigenmodes and eigenfrequencies. Eigenfrequencies: (1) 23.8 Hz; (2) 34.7 Hz; (3) 49.3 Hz; (4) 52.7 Hz; (5) 71.5 Hz; and (6) 71.7 Hz. (Eigenmode is not shown in the diagram.)

3.2.3.2. Dynamic response. To determine the dynamic response of the ship's side collision barrier due to a dynamic load of an aircraft impact both the mode superposition procedure as well as the step-by-step integration technique are used. By using mode superposition the dynamic response of the idealized structure is determined by taking into consideration the first six mode shapes; by using the step-by-step integration the time step size Δt is chosen such that $\Delta t/T_n < 0.1\ T_n$ is the natural period of the highest numbered mode that is included in the response calculation. A time step size larger than $\Delta t = 0.1\ T_n$ will not cause failure (instability), but the effect of the higher modes is 'filtered' from the predicted response. In general, with increasing time step size the solution is capable of including the effect of fewer higher frequencies.

Based on these assumptions the dynamic response analysis is carried out. The obtained results are discussed.

(a) *Dynamic displacement.* The dynamic displacements at the center of impact area are shown in fig. 7.

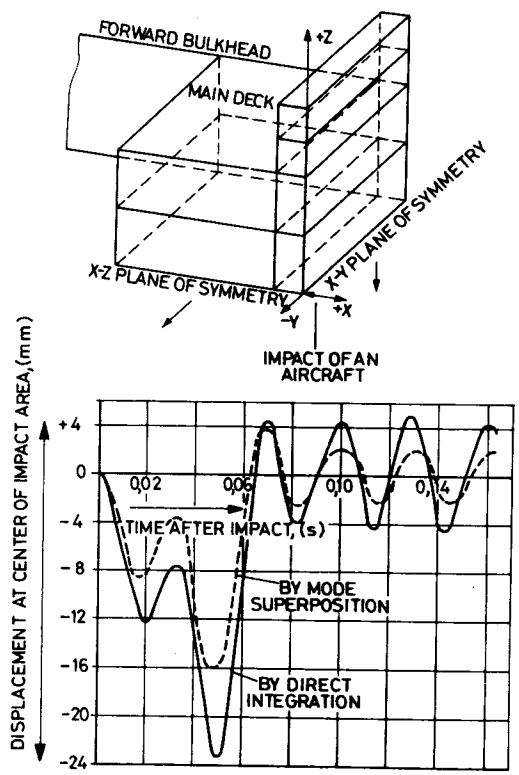

Fig. 7. Dynamic displacement at center of impact area.

It can be seen that the structure oscillates. It is noteworthy that the structure swings back at a time after impact of approximately $t = 0.02$ sec. The reason for this behavior is the resonance with the first eigenmode because the magnitude of half of the natural period ($T/2$) is approximately $T_1/2 = 0.021$ sec.

By using the mode superposition method and the step-by-step integration method the maximum values of displacement at the center of the impact area are approximately 16 and 24 mm, respectively. The ratio between these two displacements is 1.5, i.e. by using the step-by-step integration the magnitude of the maximum displacement is approximately 50% higher than by using the mode superposition method. The maximum values are reached at a time after impact of $t = 0.05$ sec. The highest impact load of 11×10^4 N (see fig. 3) acts until this time. Thereafter, the impact

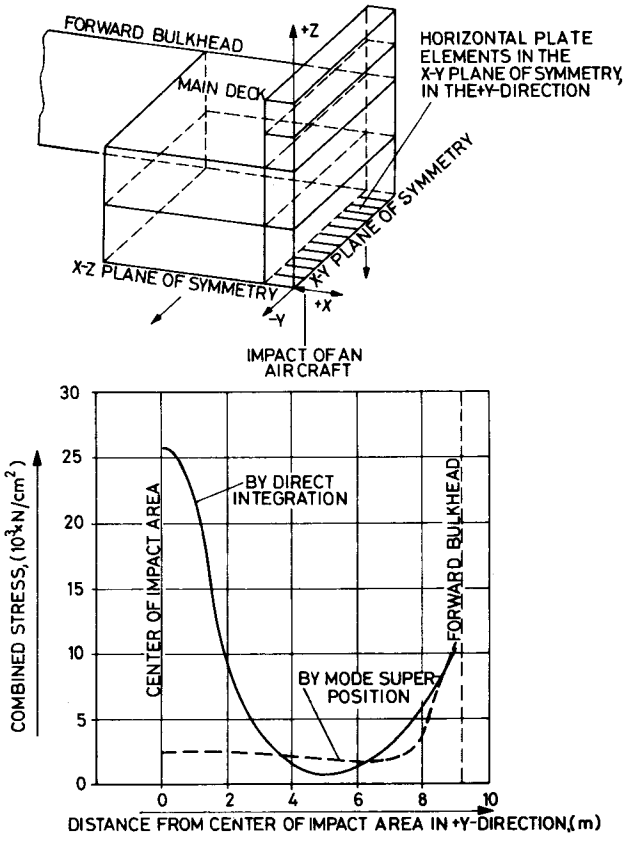

Fig. 8. Maximum combined stress in the horizontal plate elements in the $x-y$ plane of symmetry, in the $+y$ direction (time after impact $t = 0.05$ sec).

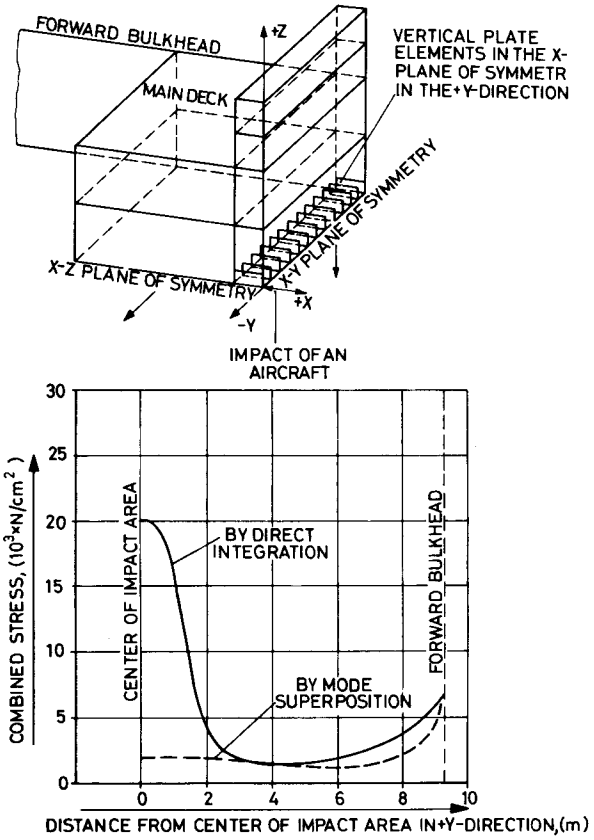

Fig. 9. Maximum combined stress in the vertical plate elements in the $x-y$ plane of symmetry, in the $+y$ direction (time after impact $t = 0.05$ sec).

load decreases linearly to zero at the duration time of impact of $t = 0.07$ sec. When the maximum displacement is reached at $t = 0.05$ sec, the structure swings back and crosses the zero axis at a time of $t = 0.065$ sec, i.e. the structure swings back before the impact load becomes zero. After that time the structure oscillates with a constant amplitude.

(b) *Stresses in the plates.* The time-dependent stress distribution in the collision barrier is very complicated. The results show that the maximum stresses in almost all the collision barrier plates occur at a time after impact of $t = 0.05$ sec. For this reason a detailed evaluation is carried out to determine the distribution of the stresses in the plates and bar steels in the $x-y$ and $x-z$ planes of symmetry (see fig. 5) at the time of $t = 0.05$ sec.

Figs. 8–15 show the curves of the combined

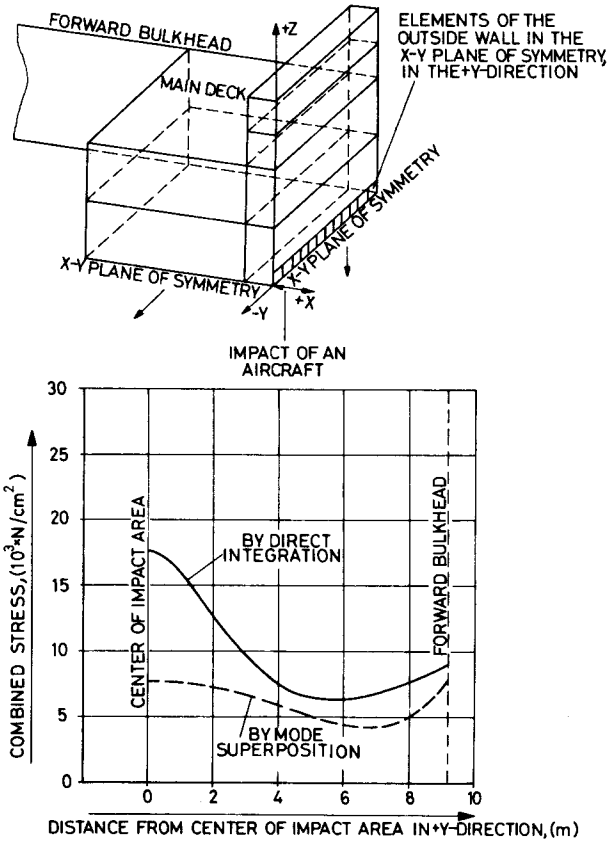

Fig. 10. Maximum combined stress in the elements of the outside wall in the $x-y$ plane of symmetry, in the $+y$ direction (time after impact t = 0.05 sec).

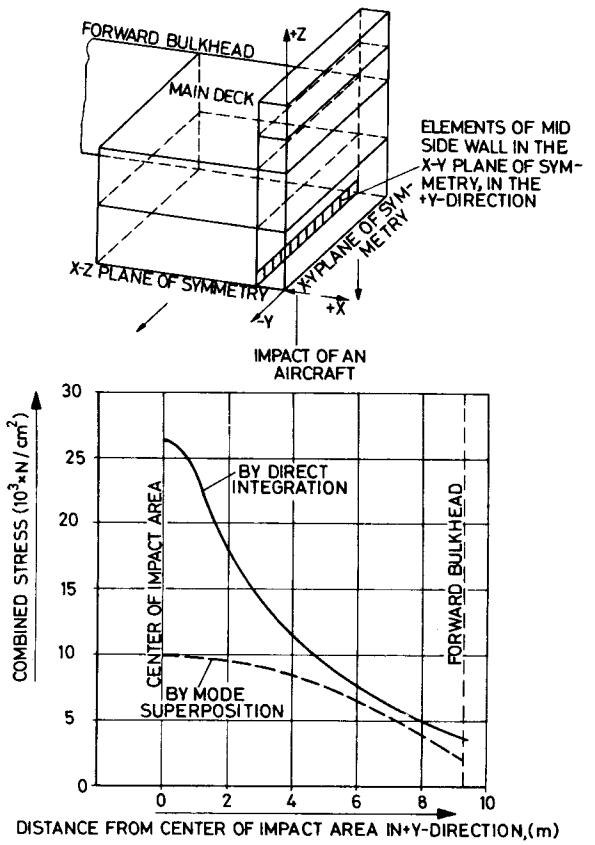

Fig. 11. Maximum combined stress in the elements of mid side wall in the $x-y$ plane of symmetry, in the $+y$ direction (time after impact t = 0.05 sec).

stress * in the individual plates of the grid structure (collision barrier) by using the mode superposition method and the direct step-by-step integration method. The general arrangement of the distribution of the maximum combined stresses in the individual elements of the grid structure is shown in fig. 16. These figures give a good survey over the distribution of the stresses in the grid structure (collision barrier).

The maximum combined stress is localized at the center of the impact area. The magnitude of this stress is approximately 26 500 N/cm^2. By using the ship steel St. 42 with a yield stress of at least 25 000 N/cm^2 [8], the magnitude of the maximum combined stress is only slightly larger than the yield stress (approximately 6%). Up to the periphery of the impact area the combined stress decreases to 20 000 N/cm^2. the decrease of the combined stress in figs. 8–10 is continued up to a distance from the center of impact area of approximately 5 m. After that distance the combined stress increases again up to the forward bulkhead. Therefore, the magnitudes of the combined stresses remain less than the magnitude of the combined stress at the center of impact area. The increase of these combined stresses is caused by the boundary conditions.

It is interesting to see that the magnitude of the combined stress at the center of the impact area is very much higher using the step-by-step integration than using the mode superposition method. The reason is that the time variation of the applied load contains significant higher frequency components, and that it is

* The combined stress is determined according to the maximum distortion energy theory.

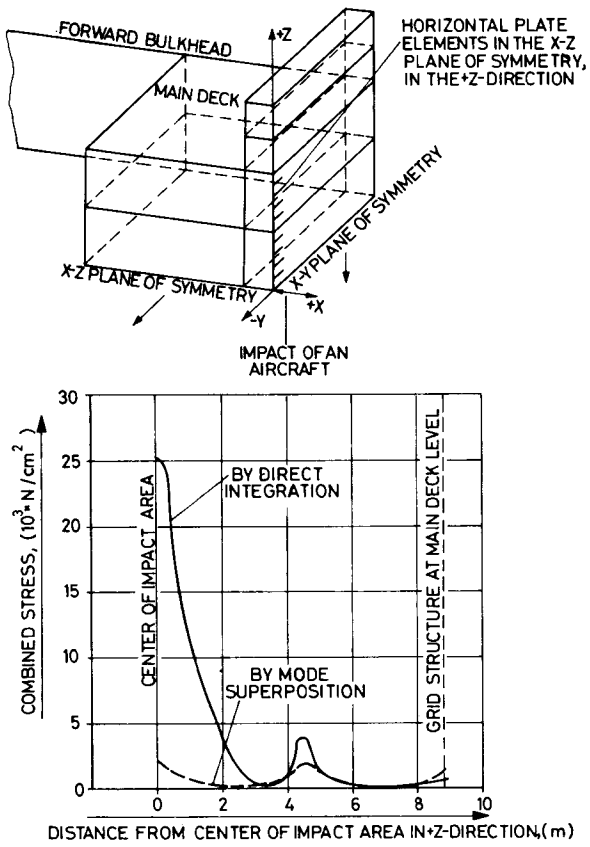

Fig. 12. Maximum combined stress in the horizontal plate elements in the $x-z$ plane of symmetry, in the $+z$ direction (time after impact $t = 0.05$ sec).

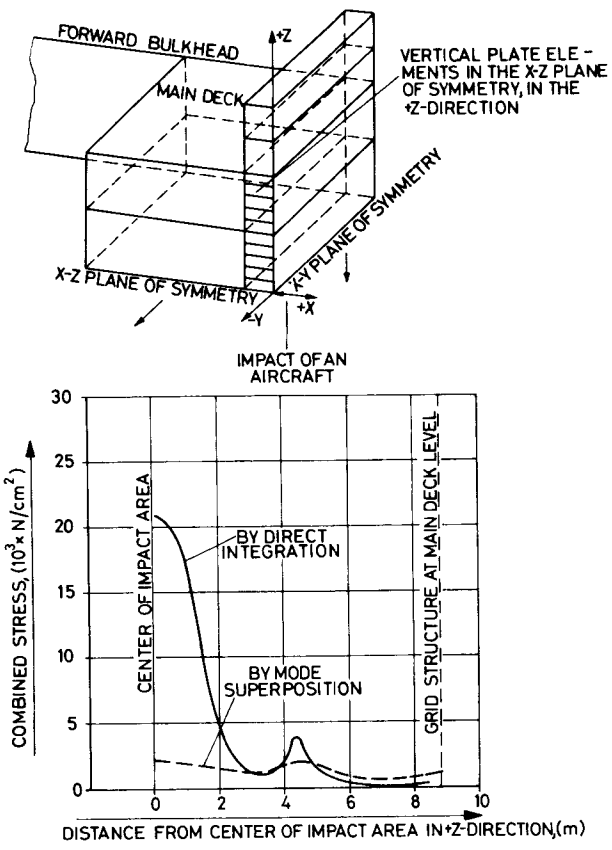

Fig. 13. Maximum combined stress in the vertical plate elements in the $x-z$ plane of symmetry, in the $+z$ direction (time after impact $t = 0.05$ sec).

necessary to include many modes of vibration to obtain adequately accurate results using mode superposition. For this present problem the number of mode shapes which is taken as the basis for using mode superposition is six (as mentioned above).

To show that the number of eigenmode shapes has an influence on the distribution of the displacements and stresses using the mode superposition method, this number of eigenmode shapes is varied. The results are shown in fig. 17. Note that by applying direct step-by-step integration and mode superposition the differences between the maximum displacements or the maximum stresses at the center of impact area decrease with increasing number of mode shapes used.

In addition, note that the curve for the maximum combined stress using the mode superposition method seems to approach a limit value when the number of eigenmodes is between 12 and 18. Therefore, without knowing the results using the step-by-step integration method, the impression could arise that an increase in the number of eigenmodes is not necessary for greater accuracy. However, for this particular case (complex structure, short impact load) this is not correct, because by increasing the number of eigenmodes using the mode superposition, the results approach the values obtained using the step-by-step method. This clearly demonstrates that the number of eigenmodes must be chosen very carefully when the mode super-

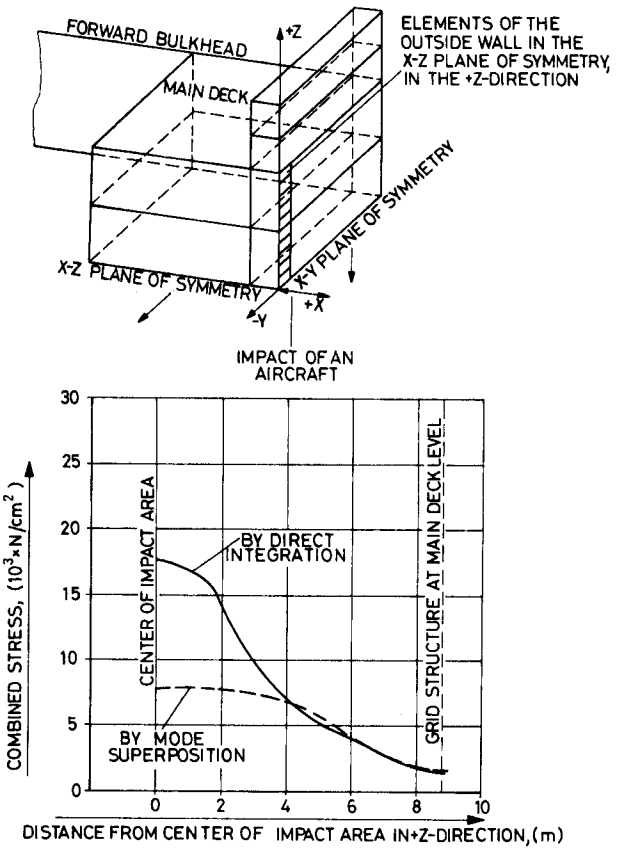

Fig. 14. Maximum combined stress in the elements of the outside wall in the $x-z$ plane of symmetry, in the $+z$ direction (time after impact t = 0.05 sec).

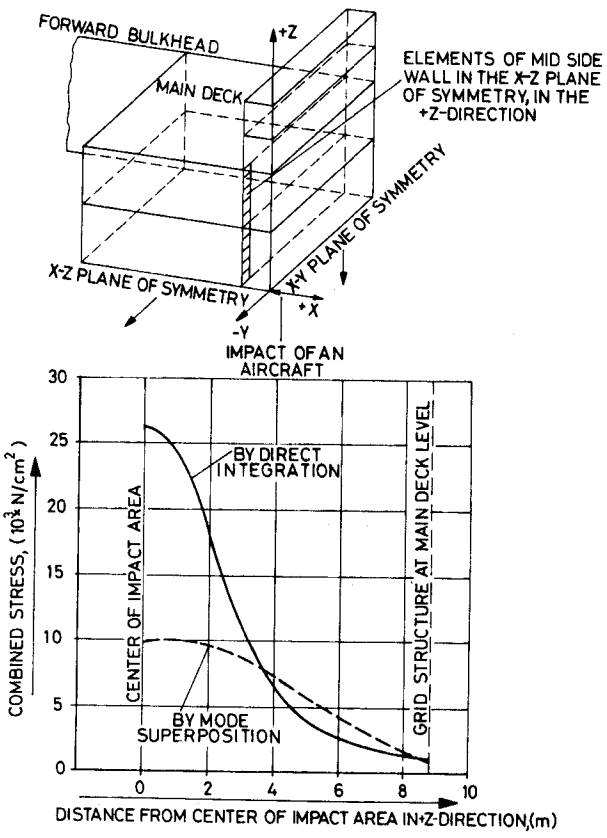

Fig. 15. Maximum combined stress in the elements of mid side wall in the $x-z$ plane of symmetry, in the $+z$ direction (time after impact t = 0.05 sec).

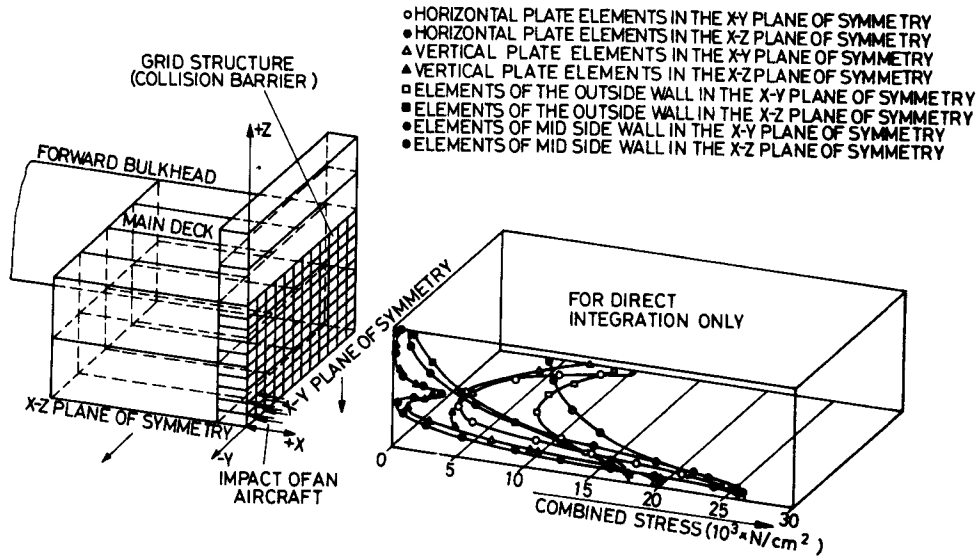

Fig. 16. General arrangement of the distribution of maximum combined stress in the individual elements of the grid structure (time after impact t = 0.05 sec).

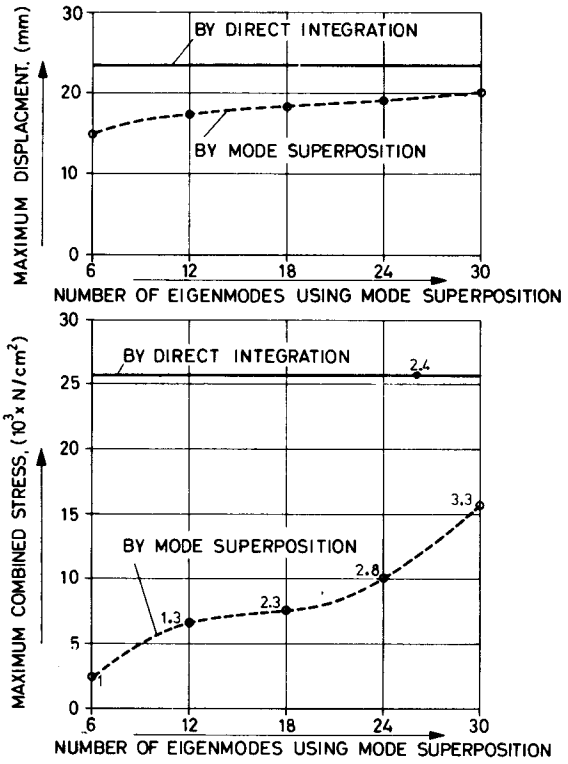

Fig. 17. Maximum displacement and maximum combined stress at center of impact area as a function of the number of eigenmode shapes (time after impact t = 0.05 sec).

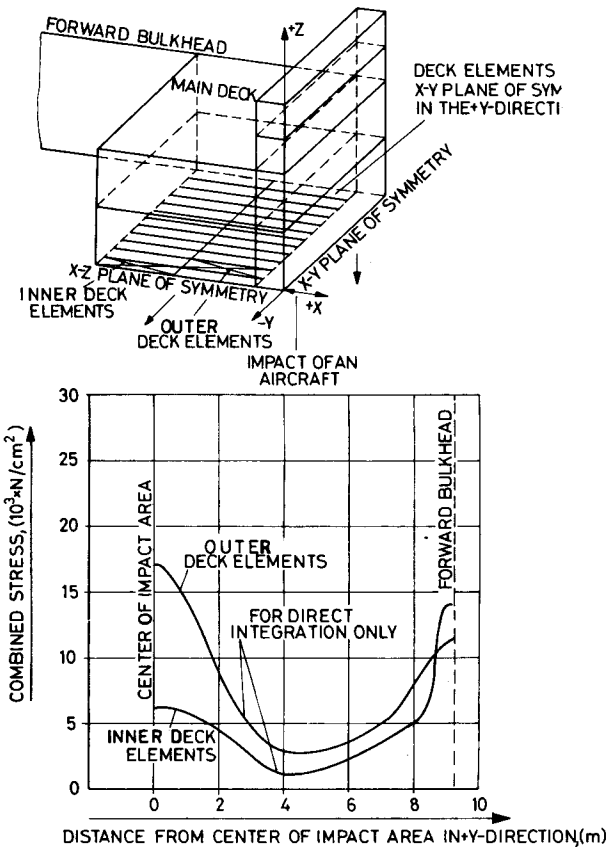

Fig. 18. Combined stress in the deck elements in the $x-y$ plane of symmetry, in the $+y$ direction (time after impact t = 0.05 sec).

position method is used to analyse complicated structures subjected to short impact loads.

The numbers at the points in the lower diagram of fig. 17 are ratios to indicate the required computer time for every individual calculation. These ratios compare the computer time of the individual calculations with the computer time of the mode superposition calculation with six mode shapes. It is noteworthy that for a calculation using mode superposition the required computer time is much higher than when using the direct step-by-step integration method if the same accuracy of the results is demanded.

Fig. 18 shows the curves for the combined stress in the deck plates in the $x-y$ plane of symmetry. The maximum combined stresses at the outer deck plates are located at the center of the impact area. To a distance of approximately 4 m from the center of the impact area the combined stress decreases to 3000 N/cm^2. After that the combined stress increases again. Therefore, the magnitude of the increased combined stress stays under those magnitudes of the combined stress at the center of the impact area. This increase of the combined stress is likewise caused by the boundary conditions.

(c) *Stresses in the bar steels underneath the deck.* The compressive stress in the bar steels underneath the deck in the $x-y$ plane of symmetry is shown in fig. 19. The maximum compressive stress is located at the forward bulkhead because the bulkhead acts as a support. The magnitude of the maximum compressive stress is approximately 23 000 N/cm^2.

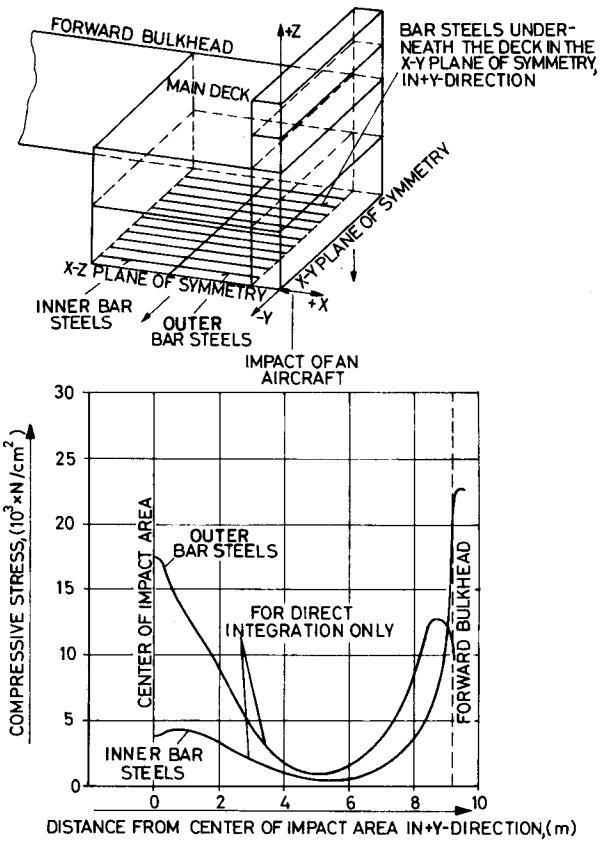

Fig. 19. Compressive stress in the bar steels underneath the deck in the $x-y$ plane of symmetry, in the $+y$ direction (time after impact t = 0.05 sec).

4. Conclusions

This structural analysis shows that the collision barrier is a sufficient safeguard against the penetration of the engine and against the failure of the structure as a result of the dynamic response to an aircraft impact. Moreover, this investigation shows that it may be necessary for the accuracy of the results to decide between the application of the step-by-step integration or the mode superposition method. The variation of the number of eigenmode shapes using the mode superposition method shows that this number has a significant influence on the accuracy of the results.

References

[1] RSK-Leitlinien für Druckwasserreaktoren, Aktenzeichen RSK/s/z – 93/4 js/schn/hn, Apr. (19
[2] K. Drittler, P. Gruner and L. Sütterlin, Zur Auslegung kerntechnischer Anlagen gegen Einwirkungen von aussen, IRS-W-7, Dez. (1973).
[3] K. Drittler, Technisch-physikalische Modelle für äussere Einwirkungen und Ableitung der Lastenannahmen, Vortrag, IRS-Fachgespräch (1974).
[4] McDonnell Douglas-F4-4E (F), Die PHANTOM II für die Luftwaffe, Flug Rev. 7 (1971) 48–51.
[5] Zeichnungs-Nr. SEP 03-03-04, Bremer Vulkan, June (1974).
[6] P. Loebel, Personal communication.
[7] J.S. Przemieniecki, Theory of Matrix Structural Analysis, McGraw-Hill, New York (1968).
[8] W. Henschke, Schiffbautechnisches Handbuch, 2. Auflage, Band 5 (1961); VEB Verlag Technik, Berlin, Seite 95.
[9] E.L. Wilson, K.J. Bathe, F.E. Peterson and H.H. Dovey, SAP/A structural analysis program for linear systems, Nucl. Eng. Des. 25 (1973 257–274.
[10] K.J. Bathe and E.L. Wilson, Solution methods for eigenvalue problems in structural mechanics, Int. J. Num. Methods Eng. 6 (1973) 213–226.
[11] R.W. Clough and K.L. Bathe, Finite element analysis of dynamic response, Proceedings 2nd US–Japan Symposium on Recent Advances in Computional Methods of Structural Analysis and Design, Berkeley, California (1972).
[12] E.L. Wilson and R.W. Clough, Dynamic response by step-by-step analysis, Proceedings Symposium on the Use of Computers in Civil Engineering, Lisbon (1962).
[13] O.C. Zienkiewicz, The Finite Element Method in Engineering Science, McGraw-Hill (1971).
[14] R.W. Clough, Analysis of structural vibrations and dynamic response, Proceedings 1st US–Japan Symposium on Recent Advances in Matrix Methods of Structural Analysis and Design, Tokyo, Japan (1968).
[15] Waffentechnisches Taschenbuch, copyright 1973 by Rheinmetall GmbH, Düsseldorf.
[16] G.R. Russel, Reactor Safeguards, Macmillan New York (1962).